A Ray Launching-Neural Network Approach for Radio Wave Propagation Analysis in Complex Indoor Environments

Leire Azpilicueta, Meenakshi Rawat, Karun Rawat, Fadhel Ghannouchi, *Fellow, IEEE* and Francisco Falcone, *Senior Member, IEEE*

***Abstract*—A novel deterministic approach to model the radio wave propagation channels in complex indoor environments reducing computational complexity is proposed. This technique combines a neural network and a 3D ray launching algorithm in order to compute wireless channel performance in indoor scenarios. An example of applying the method for studying indoor radio wave propagation is presented and the results are compared with a very high resolution fully three dimensional ray launching simulation as the reference solution. The new method allows the use of a lower number of launched rays in the simulation scenario whereas intermediate points can be predicted using neural network. Therefore a high gain in terms of computational efficiency (approximately 80% saving in simulation time) is achieved.**

***Index Terms*—3D-Ray launching, Neural Network, RF environment modeling, radio channel simulation, multipath**

I. Introduction

THE significant growth of wireless communications over the past two decades, has led to an intense interest in understanding and predicting radio wave propagation characteristics in indoor and outdoor environments. This makes it really valuable to have the capability of determining optimum base-station locations, and predicting their coverage, without carrying out a series of measurements, which are very expensive and time consuming. It is therefore fundamental to develop an effective propagation model for wireless communication, in order to provide accurate design guidelines for wireless systems.

Traditionally, empirical methods were used (such as COST-231, Walfish-Bertoni, Okumura-Hata, etc.) for initial coverage estimation [1-3]. These empirical models can give rapid results but require calibration based on measurements to provide an adequate fit of the results using regression methods. On the other hand, deterministic methods [4-10] are based on numerical approaches involving either solution of Maxwell's equations using full-wave simulation techniques, such as method of moment (MoM) and finite difference time domain (FDTD) [11], or, using geometrical approximations such as ray launching (RL) [12] and ray tracing (RT) [13]. Previously, RL and RT were both classified as ray tracing methods, although more recently both methods are distinguished. The differences are mainly due to different approaches. RL technique principle is that the transmitter launches thousands of test rays in a solid angle and the true path is determined by looking for the rays arriving at the receiver, whereas in classical RT methods the reflected paths by walls and furniture are found by computing the image of the transmitter or of the receiver. These methods are precise but are time-consuming due to inherent computational complexity. Their combination with uniform theory of diffraction (UTD) [14] is most frequently applied to radio coverage prediction [15-18]. The RT and RL models potentially represent the most accurate and versatile methods for urban and indoor, multipath propagation characterization or prediction.

Nevertheless, the computational time in the conventional ray launching, called the shooting-and-bouncing-ray (SBR) method [19], can be very large depending of the accuracy of the results. Reducing the simulation time is still a challenging problem and several acceleration techniques have been proposed in the literature to overcome this drawback. The main technique focuses on reducing the number of intersections tests of the rays with the objects in the environment. This reduction is masterly done by using geometrical algorithms based on the concept of bounding volumes [20-21]. Bounding volumes are simple geometric objects that surround the objects of the environment in a tree-like manner. The algorithm finds the intersected wall through searching in the tree generated by the bounding volumes instead of using a brute force method. Some examples are reported in [22] where the binary space is partitioned and in [23] where the volumetric space is partitioned and angular Z-buffer is used. In [24] several acceleration techniques to enhance data storing and processing are presented. Some Authors have worked on speed-up methods by splitting the 3D problem into two 2D sub-problems [25-26], while the decomposition of 3D ray propagation into 2D vertical planes is proposed in [27]. In [28-29], the environment is tessellated

Manuscript received

Leire Azpilicueta and Francisco Falcone are with the Electrical and Electronic Engineering Dept, Universidad Pública de Navarra, Pamplona, Navarra, Spain (phone: +34-948-169741; fax: +34-948-160720; e-mail: francisco.falcone@unavarra.es).

Meenakshi Rawat, Karun Rawat and Fadhel Ghannouchi are with the iRadio Laboratory, University of Calgary, Canada.

using rectangular and triangular meshes, respectively. A preprocessing and discretization of the database of the environment are proposed in [30]. Finally, two different classes of methods for speeding up ray tracing are presented in [31], aimed at reducing the size of input database and the number of rays to be handled by the algorithm.

One of the major drawbacks of the SBR method is that most of the rays emitted from the source do not reach the receiver and none of the acceleration techniques mentioned above is capable of solving this problem. However, the number of launching rays could be decreased with the aid of a trained neural network (NN) which predicts the results for intermediate rays, resulting in a significant decrease of the computational burden. In this paper, we will present a new coverage prediction method based on this idea.

The original contribution of this paper is the presentation of a new hybrid Ray Launching-Neural Network (RL-NN) technique for joint prediction of radio wave propagation using RL and NN, which is more computationally efficient as compared to the conventional RL method. This technique uses NN for modeling and storing the RL results for coverage prediction. Once NN is trained to understand RL based scenario, it allows the use of less number of launching rays in the space while power received for intermediate points can be predicted using NN. This result in computational requirement to be reduced by 80% compared with a very high-resolution fully three-dimensional (3D) RL simulation.

The paper is organized as follows. In Section II the RL method is analytically described with the geometry of the environment under the consideration. Section III presents the comparison of the neural networks considered for the new hybrid method. Measurement results are discussed in Section IV and, in Section V, simulation results and processing gain in terms of computational time are reported. Finally, conclusions are given in Section VI.

II. Ray Launching Simulation

As a starting step, the high resolution RL simulation has been done to achieve accurate results of the propagation channel. The results of this simulation are considered as a reference for comparing proposed technique with current state of art. In addition, measurements have been performed in a typical indoor scenario in order to verify the high resolution RL results. This fully 3D RL algorithm has been implemented in-house, based on Matlab™ programming environment. It is based on Geometrical Optics (GO) and Geometrical Theory of Diffraction (GTD). To complement the GO theory, the diffracted rays are introduced with the GTD and its uniform extension called as the Uniform GTD (UTD). The purpose of these rays is to remove the field discontinuities and to introduce proper field corrections, especially in the zero-field regions predicted by GO. The principle of the ray launching method is to consider a bundle of transmitted rays that may or may not reach the receiver. The number of rays considered in this bundle and the distance from the transmitter to the receiver location are the two factors determining the available spatial resolution and, hence, the accuracy of the model. A finite sample of the possible directions of the propagation from the transmitter is chosen and a ray is launched for each such direction. If a ray hits an object, then a set of a reflecting and a refracting ray is generated. If a ray hits a wedge, then a family of diffracting rays is generated. This is depicted in Fig. 1.

Rays are launched from the transmitter at an elevation angle θ and an azimuth angle Φ, as defined in the spherical coordinate system. Antenna patterns are incorporated to include the effects of antenna beam-width in both azimuth and elevation. Parameters such as frequency of operation, number of multipath reflections, separation angle between rays, and cuboids dimension are introduced. The material properties for all the elements within the scenario are also taken into account, by knowing the dielectric constant and permittivity at the frequency range of operation of the system under analysis.

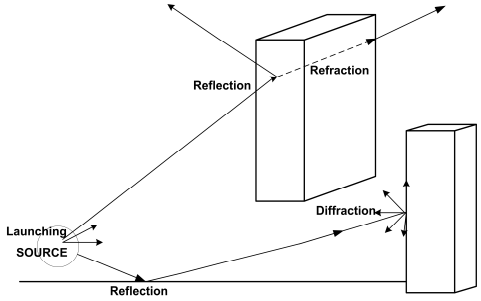

Fig. 1. Principle of operation of the 3D ray launching method implemented in-house to perform indoor coverage analysis.

Two scenarios have been considered for the analysis. First, a canonical scenario which corresponds with a small office of the second floor of the Electric and Electronic Department of the Public University of Navarre has served as the set up for the experiments. Measurements have been performed in this scenario and they have been compared with simulation. A schematic view is shown in Fig. 2 which dimensions are 3.5m x 4m x 2.5m. The small office has two tables and one bookshelf. Objects are defined as different hexahedrons in the algorithm. This basic geometric shape can conveniently be used to model any complex objects, such as tables, chairs and shelves, and placing them into the room. In a generic room, walls can be formed by windows, doors, frames, etc. Thus, to characterize the walls of a room; each discontinuity on the wall must be characterized. This will define each part of the wall like an object by its central position (x_0 , y_0 , z_0), the width in each dimension ($\Delta x, \Delta y, \Delta z$) and the material that is made. All the materials within the scenario have been taken into account for the simulation, like metal for the bookshelf, wood for the tables, and plasterboard for the walls, considering their dielectric constant and conductivity for the given frequency of operation.

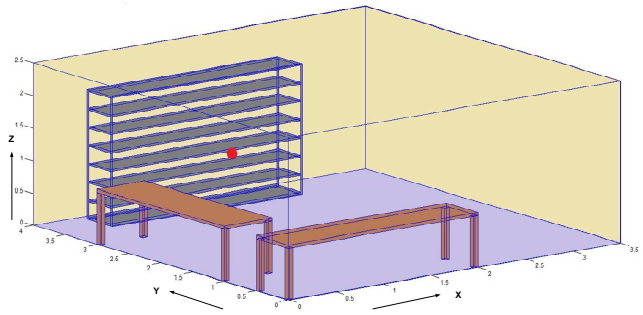

Fig. 2. Initial scenario implemented for simulation validation.

The second considered scenario is the iRadio laboratory of the University of Calgary, which has dimensions given as 8.91m by 17.85m by 3.93m. This scenario is much more complex and bigger than first one. A schematic view of the simulated scenario is depicted in Fig. 3, with the typical work stations of a laboratory. The material parameters used for both scenarios at 2.4GHz frequency are defined in Table I.

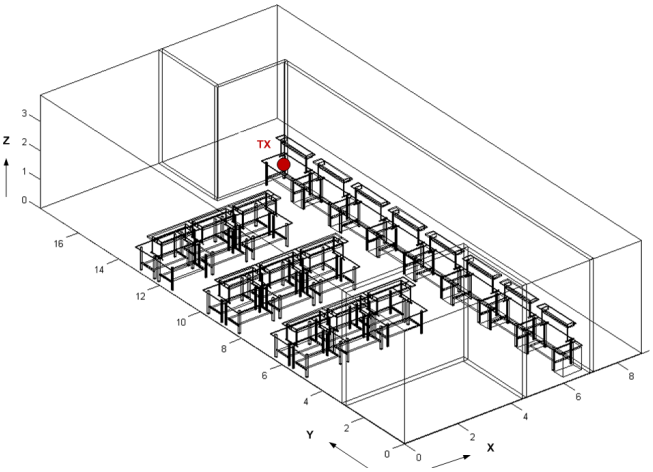

Fig. 3. Schematic view of the considered scenario for deterministic radio channel simulation.

TABLE I
MATERIAL PROPERTIES IN THE RAY LAUNCHING SIMULATION

Parameters	Air	Aluminum	Wood	Plasterboard
Permittivity (ε_r)	1	4.5	2.88	2.02
Conductivity (σ) [S/m]	0	4.10^7	0.21	0.06

Table II shows the selected parameters for the high resolution RL simulation. The transmitter and receiver antennas are omnidirectional, with 5dBi gain respectively. The angular resolution in the horizontal ($\Delta\Phi$) and vertical plane ($\Delta\theta$) for the launching rays is 0.5º. The number of reflections considered in the simulation is seven. It should be noted that this reflection number has been chosen as a result of the convergence analysis of the algorithm. Fig. 4 shows this convergence trend for different heights along Z-axis of the scenario shown in Fig. 3. The convergence trend in Fig. 4 is shown in terms of the standard deviation of received power along Y-axis for x=3m. Thus, Fig. 4 represents a measurement along YZ plane at x=3m. From Fig. 4, it can be observed that the algorithm converges for seven reflections for all the heights taken into consideration.

TABLE II
HIGH RESOLUTION RAY LAUNCHING PARAMETERS

Frequency	2.4GHz
Transmitter power	0dBm
Antenna gain	5dBi
Horizontal plane angle resolution ($\Delta\Phi$)	0.5º
Vertical plane angle resolution ($\Delta\theta$)	0.5º
Reflections	7
Cuboids resolution	12cm x 12cm x 12cm

In order to evaluate proposed hybrid RL-NN technique, a low resolution RL simulation with only four reflections has been made, storing and modeling the parameters for training the data with a NN, achieving accurate results comparable to the high resolution RL simulation as a reference technique. This comparable performance is achieved with a high efficiency gain in terms of computational time and required memory.

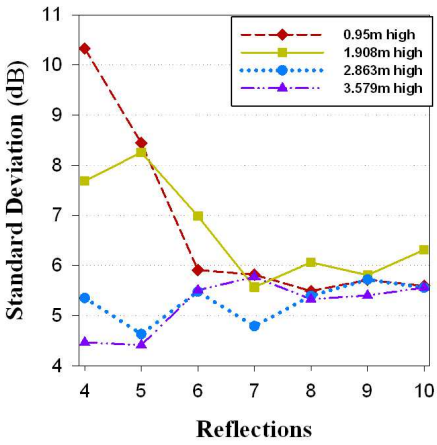

Fig. 4. Standard Deviation of Received Power for X=3m, along the Y-axis, for different heights, versus the number of reflections.

III. MULTIDIMENSIONAL NEURAL NETWORKS

For a fixed transmitter position, power decreases with respect to the distance from the transmitter and can be perceived as a nonlinear function of relative coordinates, X, Y and Z. This paper proposes the use of neural network to model this multiple-input-single-output nonlinear function. In general, neural networks works on the principle that any nonlinear function can be approximated by summation of weighted nonlinear functions [32]. A simple neural network contains nonlinear activation functions which map input signal into different nonlinear domains. These nonlinear outputs are multiplied with an appropriate weight and biased by a constant value (known as bias value) such that summation of these output domains is eventually equal to the required output.

An analogy can be perceived between the ray-tracing scheme, where the space is segmented into 3-D blocks and the power is computed for each block, and the neural network scheme where each activation function output provides nonlinear segmentation and weight/bias is adjusted to imitate computed power.

For multi-dimensional modeling, feed-forward NN (FFNN) and radial basis function NNs (RBFNN) are used extensively. FFNN neural network increases number of nonlinear segmentation using two layers containing activation functions. According to control theory, two transfer functions in series provide multiplication of transfer functions thus providing higher nonlinearity. RBFNN uses single layer with very high number of neurons with the same goal of achieving higher number of nonlinear segmentation. The working of these NNs is explained in detail in next section. In addition, the modeling capability of these NNs is assessed for the following three scenarios:

Case-I: $\Delta\phi = \pi/90$, $\Delta\theta = \pi/90$ (16200 rays).

Case-II: $\Delta\phi = \pi/180$, $\Delta\theta = \pi/180$ (64800 rays).

Case-II: $\Delta\phi = \pi/360$, $\Delta\theta = \pi/360$ (259200 rays)

Following section discusses the both NNs and their comparison from analytic point of view.

A. *Multidimensional NNs*

Feedforward Neural Network:

FFNN contains one input layer, one hidden layer and one output layer. Fig. 5(a) shows a fully connected feedforward NN. Weights are initialized randomly in the interval of [-0.8, 0.8] and converge toward their optimal values as the training proceeds.

During the forward computation, data from neurons of a lower layer (i.e., kth layer) are propagated forward to neurons in upper layer [i.e., (k+1)th layer]. The net input to any neuron, i, in any layer (k+1) is given by [32]:

$$\text{net}_i^{k+1} = \sum_{j=1}^{p} w_{ij}^{k+1} o_j^k + b_i^{k+1} \tag{1}$$

where w_{ij}^{K+1} denotes the synaptic weight connecting the j_{th} input from the previous layer to the i_{th} neuron of the present layer, P denotes the total number of neurons in the previous layers, and b_i^k denotes bias of the i_{th} neuron in the k_{th} layer. The output of neuron i at any layer (k) is calculated as:

$$o_i^k = f(\text{net}_i^k) \tag{2}$$

The output of any layer works as an input to the next layer. The output layer has a linear activation function, which sums up the outputs of hidden neurons and linearly maps them to the output. The activation function, f, chosen for two hidden layers is the hyperbolic tangent, which maps nonlinearity between -1 and 1.

The goal of training is the minimization of the error between the expected value and the actual NN that was determined in the forward computation. During the forward pass, the cost function or error energy is given by:

$$\xi = \frac{1}{2N}\sum_{n=1}^{N}\{[I_{\text{out}}(n) - \hat{I}_{\text{out}}(n)]^2 + [Q_{\text{out}}(n) - \hat{Q}_{\text{out}}(n)]^2\} \tag{3}$$

where ξ is total error, $I_{\text{out}}(n)$ and $Q_{\text{out}}(n)$ are the desired outputs, N denotes the total number of training samples, and $\hat{I}_{\text{out}}(n)$ and $\hat{Q}_{\text{out}}(n)$ are the outputs from output- layer neurons.

Starting with the output layer and moving back towards the input layer, the error term for the i_{th} neuron in k_{th} layer is calculated as:

$$\varepsilon_i^k = \begin{cases} t_i - o_i^k & k = \text{Output Layer} \\ \sum_{j=1}^{P} w_{ij}^{k+1}\delta_j^{k+1} & k = \text{Hidden Layer} \end{cases} \tag{4}$$

Where P is number of neurons in the jth layer, the local gradient, δ_i^{k+1}, for the ith neuron in the (k+1)th layer can be calculated as

$$\delta_i^k = \varepsilon_i^k f'(\text{net}_i^k) \qquad k = \text{Present Layer} \tag{5}$$

where $f'(\text{net}_i^k)$ is the derivative of the activation function.

With the aim of minimizing the error energy given in (3), the backward computation is done in batch mode to adjust the synaptic weights and biases of the network, according to the Levenberg-Marquardt algorithm [32]:

$$\Delta \boldsymbol{X} = [J^T(\boldsymbol{X})J(\boldsymbol{X}) + \mu \boldsymbol{I}]^{-1} J^T(\boldsymbol{X})\boldsymbol{e}(\boldsymbol{X}) \tag{6}$$

where μ is the gain constant, $J(\boldsymbol{X})$ is the Jacobian matrix calculated over the error matrix, $e(\boldsymbol{X})$, with respect to $\boldsymbol{X}$, where:

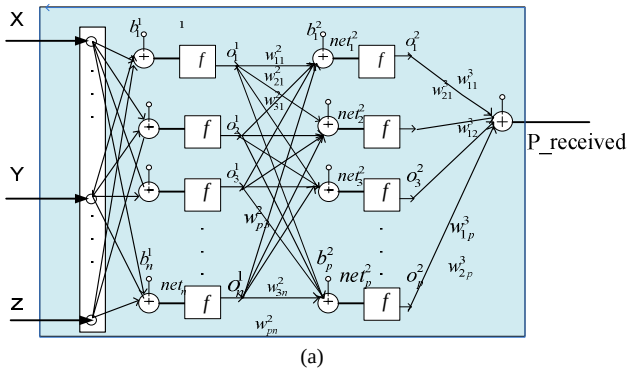

(a)

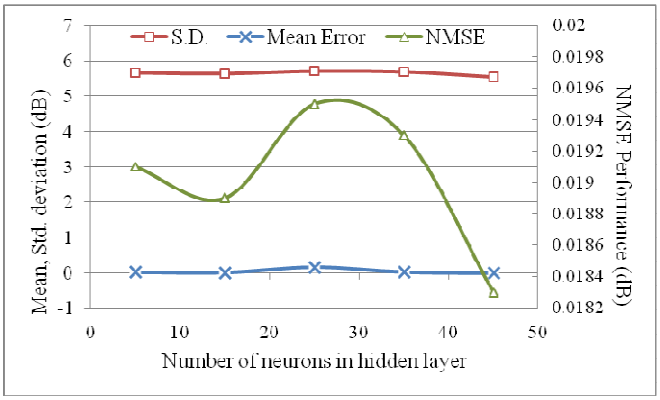

(b)

Fig.5 (a) Feedforward NN architecture. (b) Number of hidden neurons selection for case I.

$$\boldsymbol{X} = [w_{11}^1\ w_{12}^1 ... w_{nR}^1\ b_1^1 ... b_n^1 ... w_{11}^h\ w_{12}^h ... w_{nR}^h\ b_1^h ... b_n^h] \quad (7)$$

$$\boldsymbol{e(X)} = [\varepsilon_x(1)\ \varepsilon_y(1)\varepsilon_z(1)\ .....\varepsilon_x(N)\ \varepsilon_y(N)\varepsilon_z(N)]\ . \quad (8)$$

N denotes the total number of training samples, h denotes the outermost layer.

A complete description of the Levenberg-Marquardt algorithm for a three-layer feedforward NN can be found in [32], which is a numerical optimization of the Gauss-Newton method, where a small value of μ provides a Gauss-Newton solution and a very high value provides steepest descent solution. During initial iterations, μ is selected to be high (=.01); and, the algorithm converges swiftly according to steepest descent. After every iteration μ is divided by β (=10); and, after a few iterations, the algorithm takes the form of a second-order Gauss-Newton optimization, which avoids falling into local minima. The whole procedure is carried out repeatedly until the desired performance is attained or the NN starts failing the validation procedure, drifting away from the generalization criterion. The FFNN model had three neurons in input layer to account for three inputs as X, Y, Z position co-ordinates and one neuron at the output layer to account for power at that co-ordinate. Fig. 5(b) shows model performances in terms of absolute mean error, standard deviation (S.D.) and normalized mean square error (NMSE) with respect to number of neurons in hidden layer for most simple case of case-I and number of neurons in hidden layer is chosen as 15.

Radial Basis function neural network:

The topology of RBFNN is shown in Fig.6 (a), where only one layer of weights is to be adjusted. The training procedure works as follows [33]. Computational cost of learning for RBFNN is less than FFNN as neurons are added as learning continues. Initially, the hidden layer has no neuron. The nonlinear function, $\{f_i = G(\|x - t_i\|), i = 1,2....M\}$ is the Green's function defined as

$$G(\|\boldsymbol{x} - t_i\|) = \exp(-\frac{1}{2\sigma_i^2}\|\boldsymbol{x} - t_i\|^2) \quad (9)$$

which is a multivariate Gaussian function with variance σ_i^2 (spread factor), where x is the input vector and $\{t_i, i=1, 2…M\}$ are the centers of $G(.)$. The output of the j_{th} output node is given by

$$y(x) = W_{ij}.G(\|x - t_i\|) + b \quad (10)$$

where W_{ij} are the weights and b is a bias term. The smoothness of the approximation is determined. The following steps are repeated until the mean squared error falls below goal, or the number of neurons reaches to a predefined number. The goal here is set to zero.

Step-1) The network is simulated.
Step-2) The input vector with the greatest error is found.
Step-3) A neuron is added with weights equal to that vector.
Step-4) The output layer weights are redesigned to minimize error according to least mean square method. The topology requires selection of appropriate spread factor, shown in Fig. 6 (b), which is selected as 12.

B. Ray Launching modeling with NN

The implemented RL algorithm subdivides the simulation volume in uniform cuboids or blocks. In this section, each scenario in the case study is divided into a grid. The X-axis in the grid contains 146 blocks, Y-axis contains 73 blocks and Z-axis contains 33 blocks. NNs are trained for a low resolution scenario with some blocks omitted and tested for complete scenario in each case. Table III shows the modeling results for RBFNN and FFNN for the three cases. The comparisons are made in terms of total time consumption for NN training, total memory taken by processor for training including all variables as well as trained network, NMSE, standard deviation and mean error.

It can be perceived that FFNN is efficient in terms of time while RBFNN is efficient in terms of total memory required. Due to significant saving in training time, FFNN has been chosen in this paper for NN based modeling of RF trend. However, RBFNN can also be used according to memory or time requirement of any computing system because modeling performances in terms of NMSE, S.D. and absolute mean errors are almost equivalent for both NNs. It is to be noted that processing data of 1.96GB has been modeled and saved using FFNN which requires 1.6MB memory space to train and save all data in a network.

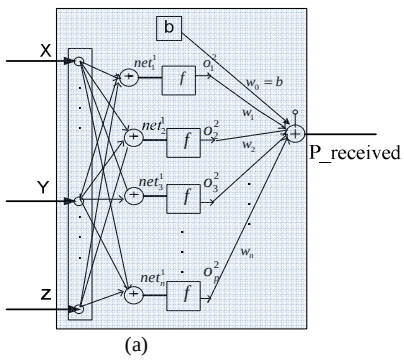

(a)

TABLE III
MODELING RESULTS FOR FFNN AND RBFNN FOR THE THREE CASES

	CASE-I		CASE-II		CASE-III	
	FFNN	RBFNN	FFNN	RBFNN	FFNN	RBFNN
Memory Consumption (MB)	1.68	1.635	1.634	1.6322	1.633	1.612
Time consumption (S)	403.46	3591.8	306.36	3491	305.53	3463.67
Std. Deviation (dB)	5.63	5.7655	9.89	10	5.586	5.6324
NMSE (dB)	.0189	.0198	.0543	.0553	.0164	.0165
Absolute Mean error (dB)	.0149	.0874	.0603	.3343	.131	.1345

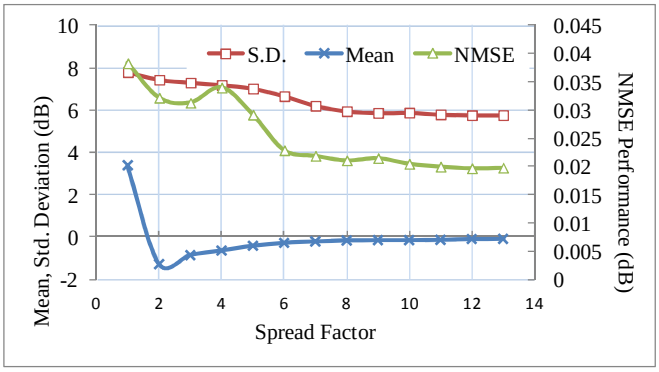

(b)

Fig. 6. (a) Radial basis function architecture (b) RBFNN spread factor impact on modeling for case I.

IV. MEASUREMENT RESULTS

In order to validate high resolution RL predictions, measurements have been performed for the first scenario depicted in Fig. 2. The wideband measurements were performed with 100MHz bandwidth at 2.4GHz frequency, a potential situation in which Wireless Local Area Network/Wireless Personal Area Network applications and services are employed. The transceivers are from Texas Instruments, specifically the CC2530 that is a true system-on-chip (SoC) solution for IEEE 802.15.4 ZigBee. The radiation pattern of the transceivers is omnidirectional with linear polarization and 0.82dBi gain. Measurements have been made with the transmitter fixed at the point *XY* (0.75m, 2m) with a height of 1.5m (the transmitter is depicted as a red point in Fig. 2). The transmitter power is 0dBm.

A portable spectrum analyzer from Agilent (N9912 Field Fox) has been used for the experiments. The measurement time at each point is 60s and the power value represented by each point is the higher peak of power shown by the spectrum analyzer for the considered bandwidth (*MaxHold* function in the 9912A Field Fox Spectrum Analyzer). Measurements have been performed for *y*=1m and *y*=2m, each 0.25m along the X-axis.

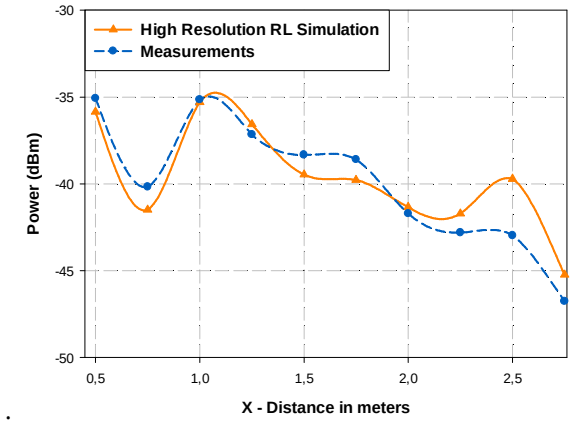

(a)

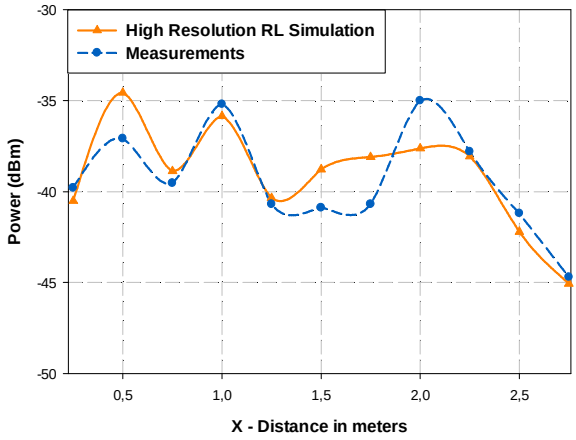

(b)

Fig. 7. Comparison simulation versus measurements along the X-axis (a) *y*=1m (b) *y*=2m

Fig. 7 shows the comparison between simulation and measurements, exhibiting good agreement with a mean error of 0.23dB with a standard deviation of 1.65dB. The differences are mainly due to approximations made in simulation within the morphological details of the definition of the scenario, which in the case of scenarios such as this one with rich multipath components, has a significant influence.

V. RL-NN Results And Discussion

Once the RL simulation code as well as the NN algorithm have been validated, both techniques are combined in order to increase computational efficiency. This validation has been performed by comparison of RL estimation (previously compared with measurements) with the obtained NN results. Fig. 8 shows the estimated received power corresponding to the measured scenario previously depicted in Fig. 2. The high resolution RL results are compared with the new joint prediction method described above as RL-NN. It can be seen that the new method RL-NN follows the trend correctly, achieving a significant reduction in computational time and resources required for simulation with this new method.

Fig. 9 and Fig. 10 show the received power at two different heights in the indoor scenario of the iRadio Laboratory (depicted in Fig. 3) for the full 3D High resolution RL and the proposed RL-NN technique which employs low resolution RL.

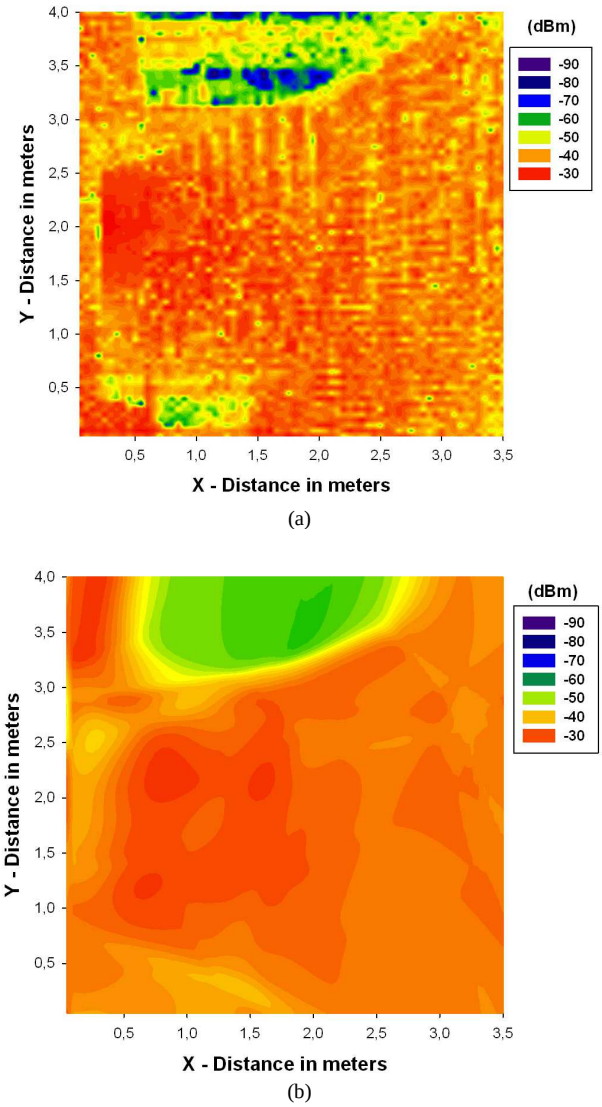

Fig. 8. Bi-dimensional planes of estimated received power for a height of 1m in scenario of Fig. 2 with (a) RL High Resolution and (b) RL Low Resolution and Neural Network.

For both heights, a good agreement between the results of the proposed method and fully 3D High resolution RL is observed. A mean error of 0.07dB and 1.19dB is observed between the results of these two techniques at 0.95m and 1.9m heights respectively. It is worth to mention that while obtaining these results, an interaction with the different elements within the indoor scenario is considered and it is observed that the material properties of the objects (see Table I) play a relevant role in the overall performance of the wireless system.

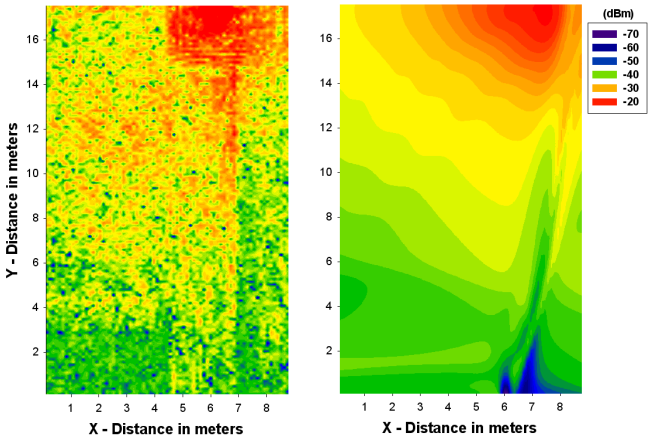

Fig. 9. Bi-dimensional planes of estimated received power for a height of 0.95m in scenario of Fig. 3 with (a) RL High Resolution and (b) RL Low Resolution and Neural Network.

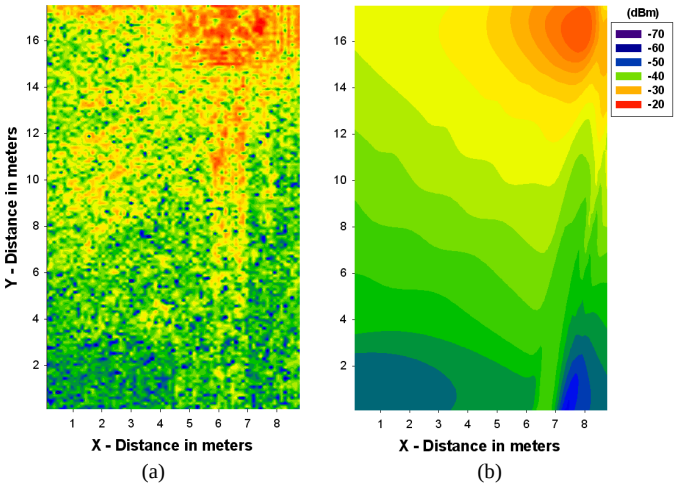

Fig. 10. Bi-dimensional planes of estimated received power for a height of 1.9m in scenario of Fig. 3 with (a) RL High Resolution and (b) RL Low Resolution and Neural Network.

The comparison between the received power along the Y-axis, for x=2m and z=0.95m height is shown in Fig. 11. It can be observed that even in high resolution RL; a lot of variations are present. This is due to multipath propagation, which is dominant phenomenon in any indoor environment and can be characterized by the temporal dispersion of the signal and the frequency dispersion because of temporal variations of the received amplitude. Thus, the RL-NN technique also follows

the trend of the high resolution RL technique.

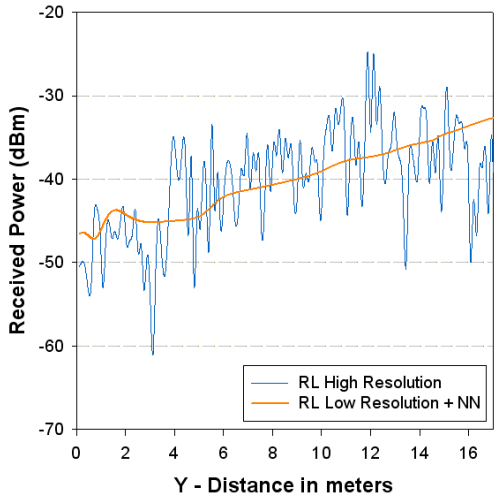

Fig. 11. Estimated received power along the Y-axis, for X=2m and Z=0.95m, for RL High Resolution and the RL+ NN proposed technique.

To illustrate the relevance of the multipath effect in the propagation channel, the power delay profile (PDP) has been predicted along the X-axis, for *y*=8m and *z*=0.95m (Fig. 12a) and for *y*=4m and *z*=0.95m (Fig. 12b). The PDP has been calculated for each cuboid along the X-axis, taking into account all the multipath components which arrive to the receiver cuboid, a similar procedure adopted in the case of PDP estimation by means of grid measurements [34, 35]. Fig. 12 represents the most significant component of the PDP for each sample point along the 8.7m of the X-axis of the scenario depicted in Fig. 3. From this figures it can be seen, there are a large number of echoes in the scenario and the significant components do not have relevant variance between both methods. Fig. 12 shows the comparison for two different cases, but the whole scenario has been characterized and compared. It is worthy to mention that the hybrid method lead to more accurate results for the first components of the multipath trajectory, as it can be seen in the depicted cases, that the tail of the PDP is not as accurate as the comparison of the first components. This is due to the fact that the proposed RL method performs the calculation in a given frequency point and hence, is inherently narrowband for a single calculation sweep. The RL+NN method provides an estimation in which a smaller amount of rays are present and therefore, the available time domain information is reduced.

To illustrate the multipath propagation properly, the RMS delay spread has been predicted for the scenario depicted in Fig. 3 for both simulation methods. The RMS delay spread has been calculated using as threshold the noise floor and it is shown in Fig. 13. It can be seen that the surrounding physical environment, as well as the geometrical position of the transmitter and the receiver, has a relevant influence in time dispersion of the mobile radio channel.

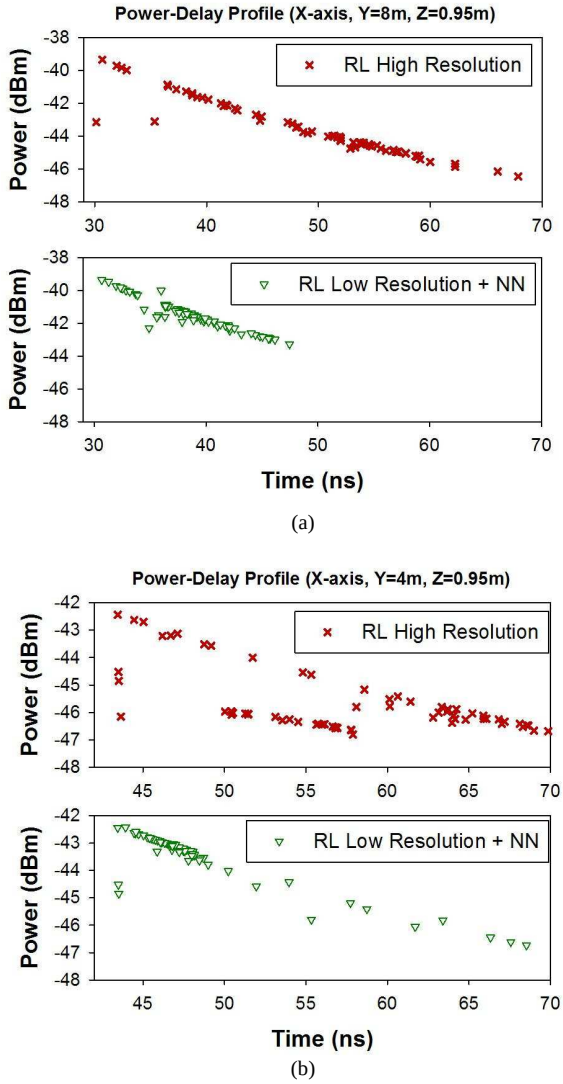

Fig. 12. Power-Delay Profile along the X-axis, for Z=0.95m, for RL High Resolution and the RL+ NN proposed technique (a) Y=8m (b) Y=4m.

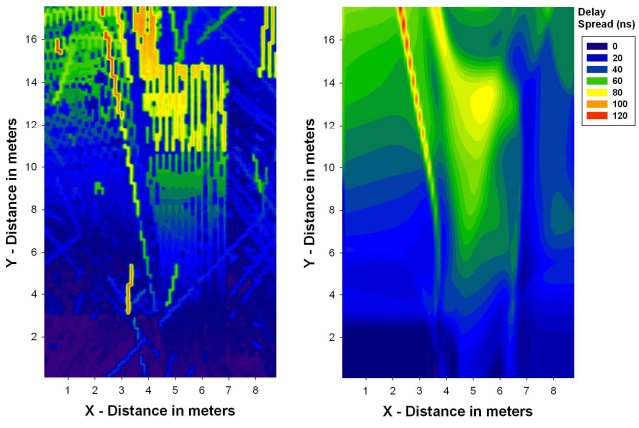

Fig. 13. Bi-dimensional planes of estimated RMS delay spread for a height of 1.9m in scenario of Fig. 3 with (a) RL High Resolution and (b) RL Low Resolution and Neural Network.

The new proposed method for coverage prediction achieves a commitment between accuracy and computational efficiency. Table IV shows the improved performance of the new method RL-NN versus the high resolution RL method in terms of computational time and energy consumption. The CPU-time savings reported include the FFNN training in the new joint approach RL-NN. The results shown present 80% reduction in terms of simulation time compared with High Resolution RL. In addition, whole 3D space data is stored in a parametric form in terms of NN weights, which lead to a 70% less memory space used in storing the massive data. The mean error acquired with the new proposed method compared with the reference solution is 0.28dB with a standard deviation of 5.96dB. These results indicate that low resolution RL results may not fully capture fast fading phenomena. Therefore, a tradeoff between computational complexity and final accuracy is present when employing this combined approach.

TABLE IV
NEW JOINT PREDICTION METHOD RL-NN

Computational time saving	80%
Computer consumption saving	70%
Mean Error	0.28dB
Standard Deviation	5.96dB

VI. CONCLUSION

In this article, a new deterministic approach for coverage prediction in complex indoor environments is presented. This technique applies a neural network (NN) for modeling and storing the ray launching (RL) results. Simulations of a real scenario have been done to compare the proposed method with a fully 3D high resolution ray launching as a reference solution. A small difference between the results of our proposed method and the fully 3D simulation is observed. However, the differences are moderate and the results are reliable for engineering purposes. The new method achieves a high gain in terms of computational efficiency, 80% reduction in simulation time and 70% reduction in used spaced memory, leading to accurate results.

ACKNOWLEDGMENT

The authors wish to acknowledge the financial support of project IIM13185.RI1 FASTER, funded by the Government of Navarra and project TEC2010-21563-C02-01 ENEIDA, funded by the Ministry of Science, Spain.

REFERENCES

[1] M. Hata, "Empirical formula for propagation loss in land mobile radio services", *IEEE Trans. Antennas and Propag*., vol. 29, no. 3, pp. 317-325, 1980.

[2] F. Ikegami, S. Yoshida, T. Takeuchi, and M. Umehira, "Propagation factors controlling mean field strength on urban streets", *IEEE Trans. Antennas and Propa*g., vol. 32, no. 8, pp. 822-829, 1984.

[3] S. Phaiboon and P. Phokharatkul, "Path loss prediction for low-rise buildings with image classification on 2-D aerial photographs", *Progress in Electromagnetics Research*, vol. 95, pp. 135-152, 2009.

[4] S. H. Lee, "A photon modeling method for the characterization of indoor optical wireless communication", *Progress in Electromagnetics Research*, vol. 92, pp. 121-136, 2009.

[5] D. J. Y. Lee and W. C. Y. Lee, "Propagation prediction in and through buildings", IEEE Trans. Veh. Tech., vol. 49, no. 5, pp. 1529-1533, 2000.

[6] S. Y. Tan and H. S. Tan, "A microcellular communications propagation model based on the uniform theory of diffraction and multiple image theory", *IEEE Trans. Antennas and Propag*., vol 44, no.10, pp. 1317-1326, 1996.

[7] A. G. Kanatas, I. D. Kountouris, G. B. Kostaras and P. Constantinou, "A UTD propagation model in urban microcellular environments", *IEEE Trans. Veh. Tech*., vol. 46, no. 1, pp. 185-193, 1997.

[8] A. G. Dimitriou and G. D. Sergiadis, "Architectural features and urban propagation", *IEEE Trans. Antennas and Propag*., vol 54, no. 3, pp. 774-784, 2006.

[9] M. Franceschetti, J. Bruck and L. J. Schulman, "A random walk model of wave propagation", *IEEE Trans. Antennas and Propag*., vol. 52, no. 5, pp. 1304-1317, 2004.

[10] J. Blas Prieto, R. M. Lorenzo Toledo, P. Fernández Reguero, E. J. Abril, A. Bahillo Martínez, S. Mazuelas Franco, and D. Bullido, "A new metric to analyze propagation models", *Progress in electromagnetics research*, vol. 91, pp. 101-121, 2009.

[11] J. W. Schuster and R. J. Luebbers, "Comparison of GTD and FDTD predictions for UHF radio wave propagation in a simple outdoor urban environment", *IEEE Antennas and Propag. Society International Symposium*, vol 3, pp. 2022-2025, 1997.

[12] S. Y. Seidel, T. S. Rappaport, "Site-Specific Propagation Prediction for Wireless In-Building Personal Communication System Design", *IEEE Transactions on Vehicular Technology*, vol. 43, no. 4, pp. 879-891, 1994.

[13] C. F. Yang, "A Ray-Tracing Method for Modeling Indoor Wave Propagation and Penetration", *IEEE Transactions on Antennas and Propagation*, vol. 46, no. 6, pp. 907-919, 1998.

[14] R. G. Kouyoumjian and P. H. Pathak, "A uniform theory of diffraction for an edge in a perfectly conducting surface", Proc. IEEE, vol. 62, no. 4, pp. 1448-1462, 1974.

[15] G. Gennarelli and G. Riccio, "A uapo-based model for propagation prediction in microcellular environments", *Progress in Electromagnetics Research B*., vol 17, pp. 101-116, 2009.

[16] H. W. Son and N. H. Myung, "A deterministic ray tube method for microcellular wave propagation prediction model", *IEEE Trans. Antennas and Propag*., vol 47, no. 8, pp. 1344-1350, 1999.

[17] A. Tayebi, J. Gómez, F. S. de Adana and O. Gutierrez, "The application of arrival and received signal strength in multipath indoor environments", *Progress In Electromagnetics Research*, vol. 91, pp. 1-15, 2009.

[18] H. B. Song, H. G. Wang, K. Hong and L. Wang, "A novel source localization scheme based on unitary esprit and city electronic maps in urban environments", *Progress In Electromagnetics Research*, vol. 94, pp. 243-262, 2009.

[19] H. Ling, R.C. Chou and S. W. Lee, "Shooting and bouncing rays: calculating the RCS of an arbitrarily shaped cavity", *IEEE Transactions on Antennas and Propagation*, 1989, vol. 37, pp. 194-205.

[20] S. Glassner, "An introduction to ray tracing", in Academic Press published by Morgan Kaufmann, 1989.

[21] J. Goldsmith, J. Salmon, "Automatic creation of object hierarchies for ray tracing", *IEEE Comput. Graph. Appl*., 1987, vol. 7, no. 5, pp. 14-20.

[22] R. P. Torres, L. Valle, M. Domingo, S. Loredo, "An efficient ray-tracing method for radiopropagation based on the modified BSP algorithm", *IEEE Vehicular Technology Conf*. (VTS 50th), Amsterdam, Netherland, vol. 4, pp. 1967-1971, September 1999

[23] M. F. Cátedra, J. Pérez, F. S. Adana, O. Gutiérrez, "Efficient ray-tracing technique for three-dimensional analyses of propagation in mobile communications: application to picocell and microcell scenarios", *IEEE Antennas and Propagat. Mag*., vol. 40, no. 2, pp. 15-28, 1998.

[24] F. Saez de Adana, O. Gutiérrez Blanco, I. González Diego, J. Pérez Arriaga, and M. F. Cátedra, "Propagation model based on ray tracing for the design of personal communication systems in indoor environments," *IEEE Trans. Veh. Technol*., vol 49, no. 6, pp. 2105-2112, Nov. 2000.

[25] J. P. Rossi and Y. Gabillet, “A mixed ray launching/tracing method for full 3-D UHF propagation modeling and comparison with wide-band measurements,” *IEEE Trans. Antennas Propag*., vol. 50, no. 4, pp. 517-523, Apr. 2002.
[26] Y. Corre, Y. Lostanlen, and Y. Le Helloco, “A new approach for radio propagation modeling in urban environment: Knife-edge diffraction combined with 2D ray-tracing,” presented at the Veh. Technol. Conf., Birmingham, AL, May 2002.
[27] G. Liang and H. L. Bertoni, “A new approach to 3-D ray tracing for propagation prediction in cities,” *IEEE Trans. Antennas Propag.*, vol. 46, no. 6, pp. 853-863, June 1998.
[28] Y. Zhengqing, M. F. Iskander, Z. Zhijun, “Fast ray tracing procedure using space division with uniform rectangular grid,” *Electronic Letters*, 36 (10), pp. 895-897, 2000.
[29] Y. Zhengqing, M. F. Iskander, Z. Zhijun, “A fast indoor/outdoor ray tracing procedure using combined uniform rectangular and unstructured triangular rids,” *IEEE Antennas Propagat. Soc. Int. Symp*., Salt Lake City, UT, vol. 2, pp. 1134-1137, July 2000
[30] R. Hoppe, G. Woelfle, and P. Wertz, “Advanced ray-optical wave propagation modeling for urban and indoor scenarios,” *Eur. Trans. Telecommun. (ETT)*, vol. 14, no. 1, pp. 61-69, Jan. 2003.
[31] V. Degli-Esposti, F. Fuschini, E. M. Vitucci, and G. Falciasecca, “Speed-Up Techniques for Ray Tracing Field Prediction Models,” IEEE Transactions on Antennas and Propagation, vol. 57, no. 5, pp. 1469-1480, May 2009.
[32] S. Haykin. Neural Networks: A Comprehensive Foundation. Upper Saddle River, NJ: Prentice-Hall, 1999.
[33] M. T. Hagan and M.B. Menhai, “Training feedforward network with the Marquardt algorithm,” *IEEE Trans. on Neural Net*., vol. 5, no. 6, pp. 989-993, 1994.
[34] M. Isaksson, D. Wisell and D. Ronnow, “Wide-band dynamic modeling of power amplifiers using radial-basis function neural networks,” *IEEE Trans. Microw. Theory Tech.*, vol. 53, no. 11, pp. 3422–3428, Nov. 2005.
[35] J.B. Andersen, K.L. Chee, M. Jacob and G.F. Pedersen "Reverberation and Absorption in An Aircraft Cabin with the Impact of Passenger", IEEE Trans on Antennas and Propagation, Vol. 60, No. 5, 2012, pp. 2472-2480, 2012
[36] S. Chiu, J. Chuang, and D. G. Michelson, “Characterization of UWB channel impulse responses within the passenger cabin of a Boeing 737-200 aircraft”, IEEE Trans Antennas Propag., vol 58, no. 3, March 2010, pp. 935–945

Leire Azpilicueta (S’13) received her Telecommunications Engineering Degree from the Public University of Navarre (UPNa), Pamplona, Spain, in 2009. In 2010 she worked in the R&D department of RFID Osés as radio engineer. In 2011, she obtained a Master of Communications held by the Public University of Navarre. She is currently pursuing the Ph.D. degree in telecommunication engineering. Her research interests are on radio propagation, mobile radio systems, ray tracing and channel modeling.

Meenakshi Rawat (S’09) received her B.Tech. degree in electrical engineering from Govind Ballabh Pant University of Agriculture and Technology, Pantnagar, Uttaranchal, India, in 2006 and her PhD from Schulich School of Engineering, University of Calgary, Calgary, AB, Canada in 2012. She was associated with Telco Construction Equipment Co. Ltd., India, from 2006-2007 and Hindustan Petroleum Corporation Limited (HPCL), India, during 2007-2008. She is now working with the iRadio Lab of the Schulich School of Engineering, University of Calgary, as a as post-doctoral-research fellow. Her current research interest is in the area of digital signal processing, nonlinear filters, artificial neural networks and microwave active and passive nonlinear circuit modeling.

Karun Rawat (M’08, S’09) received his B.E degree in electronics and communication engineering from Meerut University, UP, India, in 2002 and his Ph.D. in the Department of Electrical and Computer Engineering, Schulich School of Engineering, University of Calgary, Calgary, AB, Canada in 2012. He worked as scientist in the Indian Space Research Organization (ISRO) from 2003-2007. He had worked in iRadio Laboratory of the Schulich School of Engineering, University of Calgary, from 2012-2013 where he has been working as a post doctoral research fellow. Currently, he is assistant professor in Indian institute of Technology, Delhi. He is reviewer of several well-known journals, and his current research interests are in the areas of microwave active and passive circuit design and advanced transmitter and receiver architecture for software defined radio applications. He was also leader of University of Calgary team which won first prize and the best design award in 3rd Annual Smart Radio Challenge 2010 conducted by Wireless Innovation forum.

Fadhel M. Ghannouchi is currently a professor and iCORE / Canada Research Chair with the Department of Electrical and Computer Engineering, Schulich School of Engineering, University of Calgary, Calgary, AB, Canada, and Director of the Intelligent RF Radio Laboratory (iRadio Lab). He has held numerous invited positions with several academic and research institutions in Europe, North America and Japan. He has provided consulting services to a number of microwave and wireless communications companies. He has authored or co-authored over 500 publications. He holds ten U.S. patents with five pending. His research interests are in the areas of microwave instrumentation and measurements, nonlinear modeling of microwave devices and communications systems, design of power and spectrum efficient microwave amplification systems, and design of intelligent RF transceivers for wireless and satellite communications.

Francisco Falcone (M05, SM09) received his Telecommunications Engineering Degree (1999) and PhD in Communications Engineering (2005), both at the Universidad Pública de Navarra (UPNA) in Spain. From 1999 to 2000 he worked as Microwave Commissioning Engineer at Siemens-Italtel. From 2000 to 2008 he worked as Radio Network Engineer in Telefónica Móviles. In 2009 he co-founded Tafco Metawireless, a spin off devoted to complex EM analysis. From 2003 to 2009 he was also Assistant Lecturer at UPNA, becoming Associate Professor in 2009. His research area is artificial electromagnetic media, complex electromagnetic scenarios and wireless system analysis. He has over 280 contributions in journal and conference publications. He has been recipient of the CST Best Paper Award in 2003 and 2005, Best PhD in 2006 awarded by the Colegio Oficial de Ingenieros de Telecomunicación, Doctorate award 2004-2006 awarded by UPNA, Juan Lopez de Peñalver Young Researcher Award 2010 awarded by the Royal Academy of Engineering of Spain and Premio Talgo 2012 for Technological Innovation.